J Water Environ Nanotechnol 2026, 11(4): 491-503
10.22090/jwent.2026.2080911.2032

RESEARCH PAPER

Photocatalytic Reduction of Cr(VI) Using Carbon-Doped TiO_2/G-C_3N_4 Composite Under Visible Light Irradiation

Karrar Ayad Mohammed Jawad Deabl, Mohsen Ghorbani*

Faculty of Chemical Engineering, Babol Noshirvani University of Technology, Babol, Iran

*Corresponding Author. Email: m.ghorbani@nit.ac.ir

Article History:

Received: 2025-12-14

Revised: 2026-02-03

Accepted: 2026-02-03

How to cite this article

Deabl K A M J, Ghorbani M. Photocatalytic Reduction of Cr(VI) Using Carbon-Doped TiO_2/g-C_3N_4 Composite under Visible Light Irradiation. J Water Environ Nanotechnol 2026, 11(4): 491-503, DOI: 10.22090/jwent.2026.2080911.2032

HIGHLIGHTS

- Carbon-doped TiO_2/g-C_3N_4 nanocomposite synthesized via a simple hydrothermal route.
- Carbon doping narrowed the bandgap and improved visible-light photocatalysis.
- Up to 97.5% Cr(VI) removal achieved under visible light irradiation.
- Superoxide radicals and electrons identified as dominant active species.
- A green and cost-effective metal-free approach for Cr(VI) reduction.

ABSTRACT

In this study, hexavalent chromium (Cr(VI)) was selected as the target analyte and removed from aqueous media via a visible-light-driven photocatalytic reduction process. A carbon-doped TiO_2/g-C_3N_4 (C-TiO_2/C-g-C_3N_4) nanocomposite was synthesized through a simple and scalable hydrothermal route. The photocatalytic principle is based on efficient charge separation across a metal-free heterojunction, enabling enhanced utilization of visible light and suppression of electron–hole recombination. The structural, morphological, and optical properties of the synthesized nanocomposite were characterized using XRD, SEM, UV–vis DRS, PL, and DLS analyses, confirming the formation of a well-integrated heterostructure with a narrowed band gap of approximately 2.5 eV. Photocatalytic experiments demonstrated superior Cr(VI) reduction performance compared to individual components, achieving a maximum removal efficiency of 97.5% under optimal conditions (pH 2, initial Cr(VI) concentration of 30 mg/L, and catalyst dosage of 0.5 g/L). Kinetic analysis revealed that the reduction process followed pseudo-first-order kinetics with a high correlation coefficient (R^2 = 0.99). Recyclability tests confirmed acceptable stability over five consecutive cycles. Radical scavenger experiments identified photogenerated electrons and superoxide radicals ($\cdot O_2^-$) as the dominant reactive species, while photogenerated holes mainly acted as recombination centers. These findings highlight the potential of the C-TiO_2/C-g-C_3N_4 nanocomposite as an efficient, green, and cost-effective photocatalyst for Cr(VI) detoxification in wastewater treatment.

KEYWORDS: *Cr(VI) Reduction, Photodegradation, C-TiO_2, C-g-C_3N_4, characterization*

©2026 The Author(s). Published by the Iranian Environmental Mutagen Society. This work is licensed under the Creative Commons Attribution 4.0 International License (CC BY 4.0). To view a copy of this license, visit http://creativecommons.org/licenses/by/4.0/.

INTRODUCTION

The advancement of businesses has resulted in significant water contamination, necessitating the remediation of harmful metal contamination [1-3]. Environmental contamination from heavy metal ions poses a significant threat to ecological systems and human health [4]. In this context, chromium is a highly dangerous contaminant due to its significant solubility, mobility, and toxicity [5], originating from the effluent of electroplating, mining, petrochemical, leather industries, and metallurgical operations [6-8]. Recent research has disclosed significant pathological abnormalities in the integumentary and respiratory systems [9] as well as in the circulatory and neurological systems [8], following prolonged exposure to Cr^{6+} [10]. The World Health Organization (WHO) establishes the maximum permissible concentration of Cr(VI) in drinking water at 0.05 mg/L. [11]. Given the widespread industrial discharge and the severe health implications of Cr(VI), it is imperative to develop efficient treatment technologies capable of effectively mitigating this contaminant from aqueous environments.

Recognizing the environmental and health hazards associated with hexavalent chromium (Cr(VI)), extensive research efforts have been directed toward developing safe and cost-effective treatment strategies for Cr(VI) contaminated wastewater. Among the various reported methods, such as adsorption and biosorption [12], ultrafiltration and membrane separation [13, 14], and chemical reduction [15, 16], the reductive conversion of Cr(VI) to the less toxic trivalent form Cr(III) is particularly advantageous. This approach is widely regarded as an efficient remediation strategy due to its relatively low operational cost and minimal risk of secondary pollution, and because other methods have high cost, lack the capacity for complete eradication of toxic pollutants, or may generate secondary pollution post-treatment [17]. In recent years, photocatalysis has emerged as the optimal method for water purification due to its strong oxidative capacity against pollutants and absence of harmful by-products [18]. This technique is considered a green technology due to its utilization of unlimited solar energy. Consequently, semiconductor-based photocatalysts are thriving in the adjacent domain of solar energy harvesting and have been thoroughly investigated [19, 20].

Among several photocatalysts, TiO_2 is considered one of the most attractive due to its environmental friendliness, non-toxicity, high catalytic activity, cost-effectiveness, and chemical stability [21-23]. Commercial TiO_2 unfortunately exhibits the limitations of poor adsorption in visible light, low efficacy, and quick recombination of photogenerated carriers, significantly hindering its practical application in wastewater treatment [24]. Consequently, various modification strategies, including semiconductor coupling [25], transition metallic/non-metallic doping [26], self-assembly [27], and template preparation [28], have been devised to enhance visible light usage and photocatalytic efficacy. Non-metal doping of TiO_2 is widely regarded as an effective method for achieving a visible-light response and minimizing the recombination of photoexcited carriers [29]. Metal-free dopants modify the valence band and band gap of TiO_2 via influencing the O 2p orbital [30]. Specifically, carbon doping facilitated by carbonate groups has garnered significant interest in heterogeneous photocatalysis due to its visible light responsiveness, TiO_2 sensitization, and small bandgap [31]. The porosity and excellent electrical conductivity of the carbon support, along with the intimate interfacial electronic contact between the carbon and TiO_2 components, substantially enhance the separation of electron-hole pairs, hence increasing photocatalytic capabilities [32]. To compensate for the limitations of TiO_2, its coupling with other semiconductors—particularly those responsive to visible light—has gained increasing attention. Among these, g-C_3N_4 has emerged as a promising partner due to its compatible band structure and complementary photocatalytic properties. In recent years, g-C_3N_4, a nonmetallic semiconductor photocatalyst, has been extensively utilized in pollutant degradation, water purification, CO_2 reduction, and hydrogen production owing to its benefits of a straightforward procedure, excellent chemical stability, and an appropriate band gap (~ 2.73 eV) [33]. However, due to its limited visible light absorption spectrum and elevated rate of photogenerated electron-hole recombination, the photocatalytic efficiency of g-C_3N_4 is suboptimal [34]. Numerous methods have been employed to enhance the photocatalytic effectiveness of g-C_3N_4, including morphological structural modification [35], doping with heteroatoms [36], and coupling to different semiconductors [37]. Nonetheless, among these modification techniques, doping with non-metallic elements can augment the photocatalytic activity of g-C_3N_4 without causing secondary environmental pollution and presents remarkable application potential [38]. Carbon, a prevalent nonmetallic element in nature, possesses non-toxic and non-hazardous characteristics and is frequently utilized in semiconductor production. Consequently, carbon doping may enhance the photocatalytic activity of g-C_3N_4, and carbon self-doping possesses non-toxic and non-hazardous characteristics. Ammonium citrate is presently the subject of extensive research as a precursor abundant in nitrogen and carbon [39]. Therefore, combining carbon-doped TiO_2 and carbon-doped g-C_3N_4 into a heterostructured nanocomposite is anticipated to synergistically enhance charge separation, extend visible light absorption, and significantly improve photocatalytic efficiency. Previous studies on semiconductor heterojunction photocatalysts, such as ZnO–Cu_2O systems, have shown that efficient interfacial charge transfer and the generation of superoxide radicals play a crucial role in photocatalytic degradation under visible light irradiation [40].

During the last couple of years, carbon-doped TiO_2, g-C_3N_4,

J Water Environ Nanotechnol, 2026, 11(4): 491-503
10.22090/jwent.2026.2080911.2032

and their hybrid structures have been receiving great attention for visible-light photocatalysis in the effort to degrade organic pollutants. For instance, Ahmad et al. [41] have prepared a system of TiO_2/g-C_3N_4, which exhibited an efficiency of more than 85% in reducing Cr(VI) (20 mg/L, pH 3) under xenon lamp illumination by using 0.5 g/L of catalyst within just 90 minutes. Liu et al. [42] went one step further in the integration of NiCoP into the framework of TiO_2/g-C_3N_4 to develop a ternary Z-scheme photocatalyst. The material developed exhibited 86.2% Cr(VI) removal in two hours due to improvement in charge transport and co-catalytic activity. Zhao et al. [43], on the other hand, constructed a different heterostructure of TiO_2/α-Fe_2O_3/Fe-g-C_3N_4 prepared from iron scale waste. The photocatalyst not only removed 97.2% of Cr(VI) but also degraded levofloxacin with 93.8% efficiency in 90 min, which is attributed to efficient charge mobility and visible light utilization. Alternatively, Lu et al. [44] prepared a g-C_3N_4/Ti^{3+}-TiO_2 composite with exposed (001) and (101) facets. Their 6 wt% g-C_3N_4-loaded material realized more than 90% Cr(VI) removal under mild acidic conditions in only two hours. While these results underpin the potential of such photocatalysts, especially towards organic contaminants, their use in toxic heavy metal reduction—especially Cr(VI)—has not been explored thus far with much detail. To this date, very few studies have been done on carbon-doped TiO_2/g-C_3N_4 photocatalytic systems to investigate that purpose. This present study attempts to fill that noted gap. However, most previously reported TiO_2/g-C_3N_4-based photocatalysts rely on pristine materials, single-side modification, or incorporation of metal-based co-catalysts, which may limit charge separation efficiency or raise concerns regarding secondary metal pollution. Consequently, the potential of a fully metal-free heterojunction based on simultaneous carbon doping of both TiO_2 and g-C_3N_4 for visible-light-driven Cr(VI) reduction has not been comprehensively explored.

Therefore, to fill this research gap, the current study will focus on preparing a new photocatalyst based on carbon-doped TiO_2 incorporated with graphitic carbon nitride (g-C_3N_4), with the aim of developing an efficient and stable system that could be used for the reduction of Cr(VI) under visible light irradiation. Combining strong oxidative potential through structural tunability in carbon-doped TiO_2 with the characteristics of visible-light response and layer architecture inherent in g-C_3N_4 is likely to improve charge separation, extend light absorption, and increase photocatalytic efficiency in the composite. The material will be prepared using a simple and scalable synthesis route and characterized by XRD, FESEM, UV–vis DRS, PL, and DLS analysis in order to elucidate its structural, morphological, and optical properties. All photocatalytic experiments will be carried out by systematically monitoring the reduction of Hexavalent chromium Cr(VI) in aqueous solution under simulated solar irradiation using the synthesized composite. This not only contributes to cost-effective and environmentally friendly photocatalysts but also provides a promising approach in the context of addressing the toxic heavy metal pollution of water systems.

MATERIALS AND METHODS

Chemicals

Analytical-grade chemicals were used throughout this study without further purification. Titanium tetrachloride ($TiCl_4$, Merck, 99.9%) served as the precursor for TiO_2, while melamine (Sigma-Aldrich, 99%) was thermally condensed to prepare g-C_3N_4. Glycerol (Merck, 85%) was employed as the carbon source for doping, and ammonia solution ($NH_3 \cdot H_2O$, 35%) was used for pH adjustment during composite formation. Hydrogen peroxide (H_2O_2, 30%) acted as the oxidizing agent during photocatalytic testing. Phenol (C_6H_6O, Sigma-Aldrich, 99%) was selected as the target pollutant, and ethanol (C_2H_5OH, 99.9%) was used as solvent where needed. High-resistivity deionized water (>18 MΩ·cm) was used in every step.

Synthesis Procedures

Titanium tetrachloride was incrementally introduced dropwise into an aqueous glycerol solution while maintaining continuous agitation. The resultant sol was subjected to heating at 70 °C for 4 hours to produce a homogeneous gel, thereafter dried overnight at 80 °C and calcined at 400 °C for 2 hours to yield carbon-doped TiO_2 nanoparticles.

To introduce carbon doping, 10 g of melamine was first mixed with 3 mL of glycerol and ground into a uniform paste. The mixture was placed in a covered crucible and heated at 550 °C for 4 hours under a nitrogen atmosphere. The resultant yellowish powder, rich in internal carbon species, was collected as C-g-C_3N_4.

For the fabrication of the C-TiO_2/C-g-C_3N_4 Nanocomposite, Equal masses of the previously synthesized C-TiO_2 and C-g-C_3N_4 were dispersed in a mixture of ethanol and ammonia solution. The suspension was ultrasonicated and then subjected to hydrothermal treatment at 150 °C for 24 hours. After cooling, the product was washed, dried at 70 °C, and calcined at 500 °C for 2 hours to enhance crystallinity and improve interfacial contact between the two components.

Characterization

To comprehensively understand the structural, morphological, and optical features of the synthesized photocatalysts, several analytical techniques were employed. X-ray diffraction (XRD) was utilized to investigate the crystallinity and phase composition of the samples. Measurements were performed over the 2θ range of 20°–80° using Cu Kα radiation (λ = 1.5406 Å), and crystallite sizes were estimated using the Scherrer equation. The surface morphology and particle dispersion were examined by scanning electron microscopy (SEM), which provided visual insights into particle

shape, size distribution, and the interfacial contact between TiO_2 and g-C_3N_4 in the composite structure. The optical absorption properties of the materials were analyzed via UV–Visible diffuse reflectance spectroscopy (DRS). The obtained spectra were used to estimate the bandgap energy of the photocatalysts using the Tauc plot method, providing critical information on their light-harvesting capabilities under visible light irradiation. Furthermore, dynamic light scattering (DLS) research was conducted to ascertain the hydrodynamic particle size distribution of the produced photocatalysts in aqueous suspension.

Photocatalytic Reduction of Cr(VI)

The photocatalytic reduction experiments were conducted to evaluate the ability of the synthesized C-TiO_2/C-g-C_3N_4 nanocomposite to reduce hexavalent chromium (Cr(VI)) under visible light. In a standard test, 50 mg of the photocatalyst was suspended in 100 mL of an aqueous solution having 20 mg/L of Cr(VI), prepared using potassium dichromate ($K_2Cr_2O_7$) as the chromium source. The mixture was magnetically agitated in the dark for 30 minutes before light exposure to achieve adsorption-desorption equilibrium.

Visible light irradiation was supplied by a 300 W xenon lamp fitted with a cut-off filter ($\lambda > 400$ nm). Aliquots were taken at regular intervals (30, 60, 90, 120, and 150 minutes), centrifuged, and examined to ascertain the concentration of residual Cr(VI) using a UV–Vis spectrophotometer at 540 nm after complexation with diphenylcarbazide.

The reduction efficiency was calculated using the following formula (1):

$$\%RE = \frac{C_0 - C}{C_0} \times 100 \quad (1)$$

where C_0 represents the initial Cr(VI) concentration, and C_t is the concentration at time t.

Kinetic behavior was assessed by applying the pseudo-first-order model (equation 2):

$$\ln(C/C_0) = -k_1 \cdot t \quad (2)$$

where k_1 represents the apparent rate constant.

Kinetic behavior was also evaluated using the pseudo-second-order model. This model posits that the rate-limiting step may entail chemical adsorption, wherein the concentrations of Cr(VI) and the accessibility of active sites on the photocatalyst surface are crucial factors. The linearized representation of the pseudo-second-order equation is articulated as 3:

$$\frac{t}{C} = \frac{1}{k_2 C_0^2} + \frac{t}{C_0} \quad (3)$$

where k_2 is the pseudo-second-order rate constant, C_0 represents the initial concentration of Cr(VI), and C is the concentration at time t. A plot of $\frac{t}{C}$ versus t is expected to yield a straight line if the system follows second-order kinetics.

To better understand the operational efficiency, the influence of critical parameters such as solution pH, initial Cr(VI) concentration, catalyst dosage, and irradiation time was systematically explored. The role of pH was systematically examined by adjusting the initial pH of the Cr(VI) solution to different levels before irradiation, as proton availability is known to influence the photocatalytic reduction process.

All experiments were performed in triplicate, and data are presented as mean ± standard deviation.

RESULTS

Characterization

The surface morphology of the synthesized C-TiO_2, C-g-C_3N_4, and their nanocomposite was examined using SEM, as depicted in Fig. 1. Fig. 1a illustrates C-g-C_3N_4 (magnification of 7,500×), showcasing a layered, sheet-like structure that is characteristic of thermally polymerized graphitic carbon nitride. These delicate, wrinkled nanosheets showcase a significant surface area, enhancing their ability to capture light and offering numerous active sites for photocatalytic processes. Fig. 1b represents C-TiO_2 (magnification of 15,000×), showing densely packed and agglomerated nanoparticles with a relatively rough texture. The granular morphology suggests successful carbon doping and a high surface density, which facilitates increased photon interaction and reactive species generation during photocatalysis. Fig. 1c depicts the C-TiO_2/g-C_3N_4 nanocomposite, where TiO_2 nanoparticles are uniformly anchored onto the g-C_3N_4 sheets. This thoughtfully designed hybrid structure suggests a robust connection at the interface of the two components. The uniform distribution of TiO_2 within the g-C_3N_4 matrix not only facilitates better charge separation but also boosts the absorption of visible light. Such morphology is crucial for constructing an effective heterojunction, thereby promoting better photocatalytic efficiency in the reduction of Cr(VI). The SEM observations confirm the successful synthesis and integration of the nanocomposite components, supporting the improved functional performance in subsequent photocatalytic applications.

Fig. 2 shows the XRD examination results for C-g-C_3N_4, C-TiO_2 nanoparticles, and their nanocomposite. In the case of C-TiO_2, peaks of 27.21°, 35.9°, 43.75°, 54.07°, 56.51°, and 63.63° have been identified at 2θ and attributed to (101), (004), (200), (105), (211), and (204) crystallographic planes, respectively. These reflections correspond exactly to the anatase phase of TiO_2, as validated by JCPDS No. 89-4921. The height and intensity of all these peaks confirm excellent crystallinity, which is an essential prerequisite for having superior photocatalytic

J Water Environ Nanotechnol, 2026, 11(4): 491-503
10.22090/jwent.2026.2080911.2032

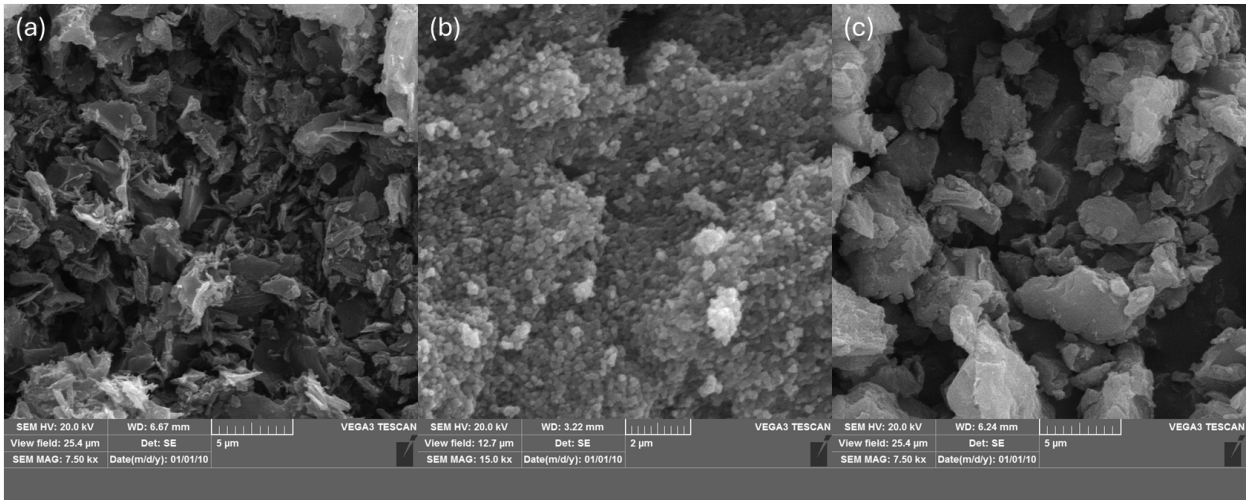


Fig. 1 SEM images of a) C-g-C_3N_4, b) C-TiO_2, and c) Nanocomposite

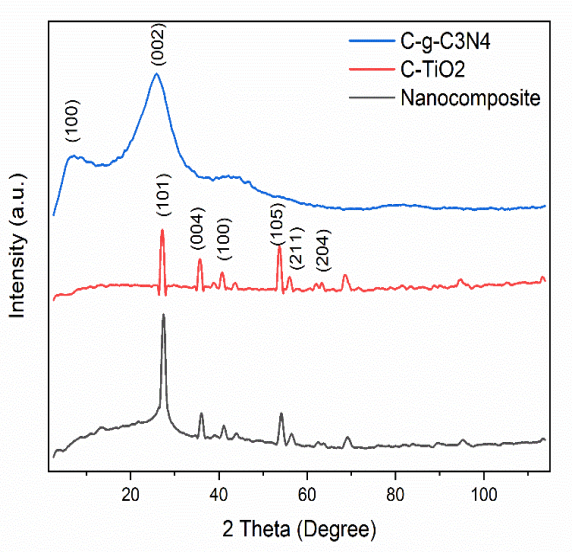


Fig. 2. XRD patterns of C-TiO_2, C-g-C_3N_4, and the C-TiO_2/C-g-C_3N_4 nanocomposite.

activity. The anatase phase exhibits more chemical stability and enhanced electron transfer efficiency under light irradiation [32, 45].

C-g-C_3N_4 presents two characteristic peaks. The first peak at about 9.33° corresponds to the (100) crystal plane, reflecting the in-plane structural periodicity of the tri-s-triazine units. On the other hand, the peak at around 25.9° can be attributed to the (002) plane, which reflects the interlayer stacking of aromatic segments in g-C_3N_4. The above two peaks confirm the formation of the layered, graphitic-like structure, helpful for the enhancement of visible light absorption and charge transfer during the photocatalytic process [46].

In the XRD pattern of the final C-TiO_2/C-g-C_3N_4 nanocomposite, the diffraction features arose from both TiO_2 and g-C_3N_4, confirming their successful integration. No additional peaks were observed, showing that no impurities or undesirable phases were introduced during the synthesis. The combined structural features suggest the formation of a heterojunction between C-TiO_2 and C-g-C_3N_4, which can facilitate better charge separation and visible light utilization. These properties are essential for enhancing the photocatalytic activity of the composite, especially for environmental

remediation purposes such as heavy metal reduction or organic pollutant degradation.

The optical behavior of the prepared samples was examined through DRS, and the corresponding band gap energies were estimated using Tauc plots, as illustrated in Fig. 3. In the DRS spectra (Fig. 3a), C-TiO_2 displays a steep increase in reflectance in the UV region and a sharp absorption edge near 400 nm, indicating its limited ability to utilize visible light due to its wide bandgap. In contrast, C-g-C_3N_4 and the C-TiO_2/C-g-C_3N_4 nanocomposite show significantly lower reflectance values across the visible range (400–800 nm), indicating improved absorption of visible light. This enhancement can be attributed to the narrower band gaps of g-C_3N_4 and the synergistic effects induced by composite formation. The Tauc plots obtained from the reflectance spectra (Fig. 4b) were utilized to compute the optical band gaps employing the Kubelka–Munk function. The bandgap of C-TiO_2 was approximated at ~2.65 eV, diminished from the standard 3.2 eV of pure anatase [47], attributable to carbon doping that creates localized mid-gap states and alters the electrical structure. The bandgap of C-g-C_3N_4 was determined to be approximately 2.45 eV, aligning with prior studies and validating its inherent capacity to absorb visible light. The nanocomposite had an intermediate bandgap of approximately 2.50 eV, suggesting that the combination of both components results in advantageous electronic interactions. The decrease in bandgap energy of the nanocomposite indicates that the composite structure enhances light harvesting and induces a red shift in absorption, allowing excitation at longer wavelengths. Moreover, the close interface interaction between C-TiO_2 and C-g-C_3N_4 facilitates charge transport across the heterojunction and mitigates the recombination of photoinduced electron-hole pairs. These heterojunctions are recognized for generating internal electric fields at the interface, facilitating charge separation and prolonging their lives. The charge separation mechanism, along with improved visible-light absorption, substantially enhances the photocatalytic efficacy of the composite in Cr(VI) reduction.

The PL spectra of nanoparticles and the C-TiO_2/C-g-C_3N_4 nanocomposite (Fig. 4 a) offer important insights into the recombination behavior of photogenerated charge carriers. The spectra were captured within the range of 500 to 600 nm, a region where both C-g-C_3N_4 and carbon-doped TiO_2 commonly display emission resulting from electron-hole recombination. Among the individual components, C-g-C_3N_4 exhibited a notably strong photoluminescence emission, suggesting an increased rate of recombination for photo-induced charge carriers. In contrast, C-TiO_2 showed a slightly reduced emission intensity, indicating a potential enhancement in charge separation efficiency. This improvement may be attributed to carbon doping, which enhances electronic conductivity and promotes defect formation. The nanocomposite exhibited the lowest photoluminescence intensity when compared to both pristine C-TiO_2 and C-g-C_3N_4. The notable reduction in PL emission indicates the establishment of a highly effective heterojunction structure between the two components, facilitating a more efficient separation of photogenerated electron-hole pairs. The decrease in recombination leads to longer carrier lifetimes, which in turn raises the likelihood of their involvement in redox reactions, thereby improving the photocatalytic activity of the nanocomposite. The results of this study provide additional evidence for the collaborative interaction between C-TiO_2 and C-g-C_3N_4, highlighting the composite's potential as an effective photocatalyst for environmental remediation under visible light.

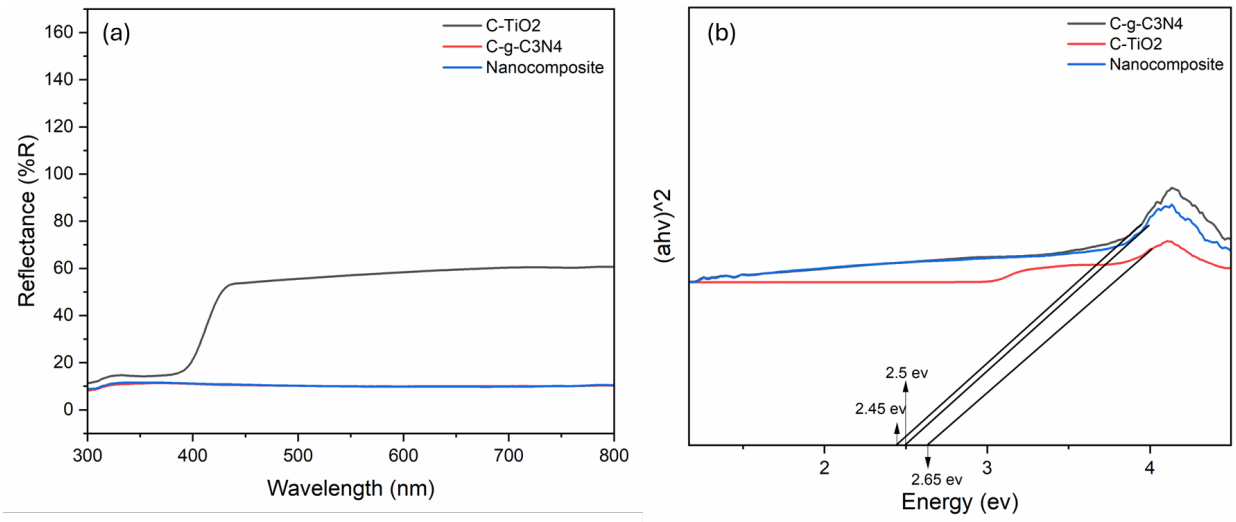


Fig. 3. (a) DRS of C-TiO_2, C-g-C_3N_4, and the C-TiO_2/C-g-C_3N_4 nanocomposite, and **(b)** corresponding Tauc plots used for optical band gap estimation.

J Water Environ Nanotechnol, 2026, 11(4): 491-503
10.22090/jwent.2026.2080911.2032

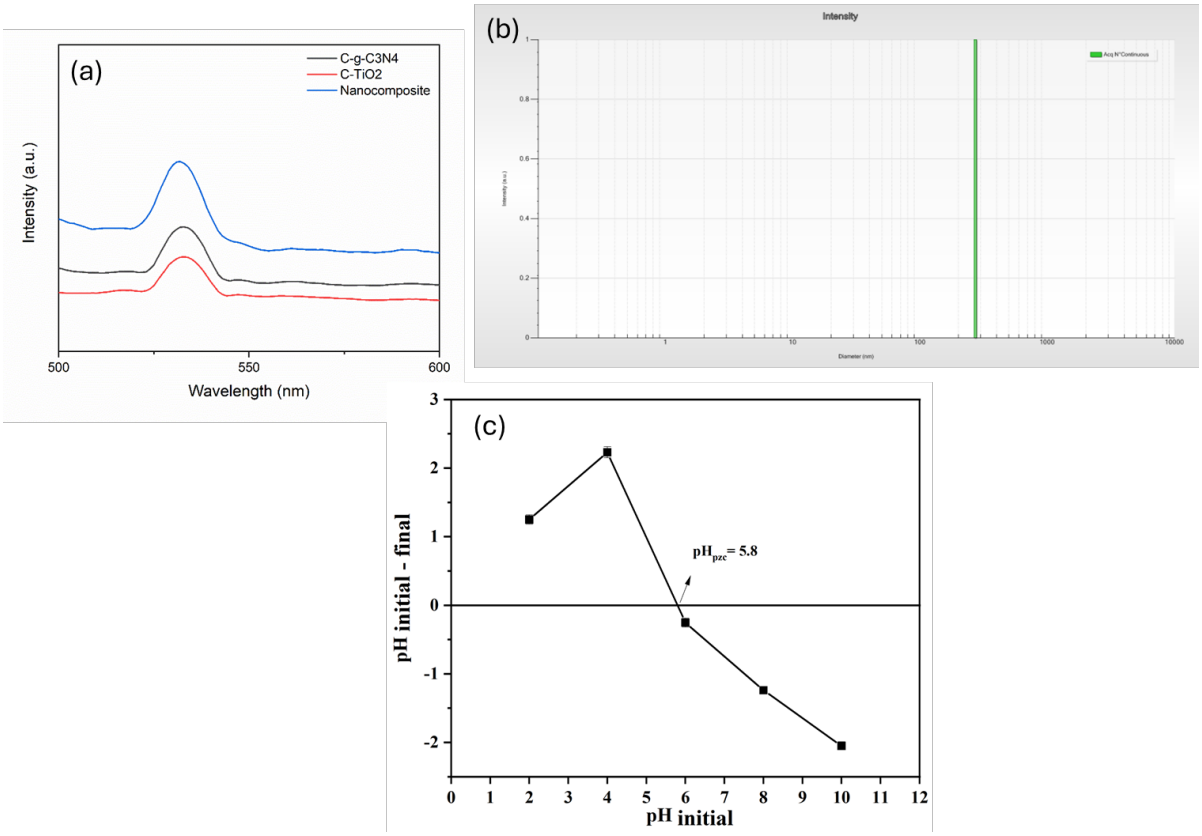


Fig. 4. (a) PL spectra of C-TiO_2, C-g-C_3N_4, and the C-TiO_2/C-g-C_3N_4 nanocomposite, **(b)** DLS particle size distribution of the nanocomposite, and **(c)** point of zero charge (pH_{PZC}) of the C-TiO_2/C-g-C_3N_4 nanocomposite using the pH drift method

DLS was utilized to measure the particle size distribution of the C-TiO_2/g-C_3N_4 nanocomposite. As shown in Fig. 4 b, the particles displayed a sharp, single peak with a mean intensity diameter of approximately 271.48 nm. The D10, D50, and D90 values were all equal to 271.48 nm, confirming that nearly all particles in the sample had the same size. This strongly indicates a monodisperse system with excellent uniformity and no signs of aggregation. The detected size of 273.84 nm, with a high intensity value (0.94), supports the conclusion that the nanocomposite particles are well-dispersed and stable in solution. This consistent particle size distribution is important because it contributes to better photocatalytic activity by providing a larger surface area and improving light absorption. The absence of multiple peaks in the DLS graph also confirms that the synthesis process successfully prevented particle agglomeration, resulting in a stable colloidal dispersion.

The surface charge behavior of the C-TiO_2/C-g-C_3N_4 nanocomposite was evaluated using the pH drift method to determine its point of zero charge (pH_{PZC}). As shown in Fig. 4c, the variation of ΔpH ($pH_{final} - pH_{initial}$) as a function of the initial pH indicates a clear intersection with the zero line at pH 5.8, which corresponds to the pH_{PZC} of the nanocomposite. At pH values lower than pH_{PZC}, positive ΔpH values are observed, implying that the surface of the photocatalyst becomes positively charged. In contrast, at pH values higher than pH_{PZC}, negative ΔpH values dominate, indicating a negatively charged surface. This pH-dependent surface charge behavior plays an important role in governing the interaction between the photocatalyst and aqueous Cr(VI) species. Under acidic conditions (pH < pH_{PZC}), the positively charged surface of the nanocomposite favors electrostatic attraction toward negatively charged Cr(VI) species, such as $HCrO_4^-$ and $Cr_2O_7^{2-}$, thereby facilitating adsorption and subsequent interfacial electron transfer. Conversely, at higher pH values (pH > pH_{PZC}), electrostatic repulsion between the negatively charged surface and Cr(VI) anions can hinder adsorption, which is expected to adversely affect the reduction efficiency. Therefore, the determined pH_{PZC} value of 5.8 provides a fundamental explanation for the strong pH dependence observed in the photocatalytic reduction of Cr(VI), and it establishes a physicochemical basis for the enhanced photocatalytic performance under acidic conditions discussed in the following section.

Photocatalytic Cr(VI) Reduction

Photocatalytic reduction of Cr(VI) by individual nanoparticles, including TiO_2, C-TiO_2, g-C_3N_4, and C-g-C_3N_4, was conducted under the same experimental conditions: Cr(VI) = 50 mg/L, catalyst dose = 0.3 g, pH = 2. Then, its efficiencies were compared with those of the C-TiO_2/C-g-C_3N_4 nanocomposite, as illustrated in Fig. 5 a. The Cr(VI) removal efficiency of the resultant nanocomposite was 78.4%, which was considerably higher than that of its individual photocatalysts. In comparison, under the same conditions, bare TiO_2 showed relatively low photocatalytic activity, with a total Cr(VI) removal below 25%, mainly because of its wide bandgap (~3.2 eV), which limits its light absorption to the UV region and negatively impacts visible-light-driven photocatalytic performance. C-TiO_2 prepared by this method showed an improved performance of 52% in total removal efficiency, thanks to enhanced absorption in the visible light range by bandgap narrowing and improved charge separation induced by carbon doping. The doping created localized states within the TiO_2 band structure, which, on one hand, allowed excitation by lower-energy light and, on the other hand, suppressed recombination. It was found that pristine g-C_3N_4 has higher photocatalytic efficiency compared to bare TiO_2, reaching 38% total Cr(VI) removal. The narrow bandgap (~2.7 eV) allows effective absorption of visible light. However, its high electron-hole recombination rate seriously limits its photocatalytic efficiency. C-g-C_3N_4 exhibited a slightly higher photocatalytic performance, up to 60% total removal. Carbon doping introduced defective sites, which enhanced the mobility of charges; the recombination rate of photogenerated carriers decreased and thus enhanced the visible-light photocatalytic activity. Among all samples, the C-TiO_2/C-g-C_3N_4 nanocomposite exhibited the highest efficiency. The improved efficiency can be understood in terms of a synergistic interaction between C-TiO_2 and C-g-C_3N_4 that could lead to better charge transfer through the heterojunction interface and thus inhibit electron-hole recombination. Furthermore, the complementary absorption range of sunlight (UV region for TiO_2 and visible region for g C_3N_4) broadens the usage of sunlight in the composite, which could account for the increased photocatalytic efficiency under visible light. These results altogether confirm that the fabrication of a carbon-doped heterojunction of TiO_2 and g C_3N_4 offers an efficient pathway toward enhanced reduction of Cr(VI), which is attributed to enhanced light absorption, efficient charge separation, and reduced recombination dynamics.

The effect of solution pH on photocatalytic Cr(VI) reduction was studied at different pH values (2, 4, 6, 8, and 10) while keeping other parameters constant (Cr(VI) = 50 mg/L, catalyst dose = 0.3 g/L). As shown in Fig. 5b, the removal efficiency of Cr(VI) is significantly influenced by the solution pH. The highest reduction efficiency was achieved at pH 2, with 78.4% Cr(VI) removal after 30 minutes of dark adsorption followed by 150 minutes of visible light irradiation. This enhanced performance under acidic conditions can be explained by the combined effects of Cr(VI) speciation and the surface charge behavior of the photocatalyst. At low pH values, particularly at pH 2, Cr(VI) predominantly exists as $HCrO_4^-$ and $Cr_2O_7^{2-}$ species, which possess higher reduction potentials and can be more readily reduced. Moreover, based on the determined pH_{PZC} value (5.8), the surface of the C-TiO_2/C-g-C_3N_4 nanocomposite is positively charged under acidic conditions ($pH < pH_{PZC}$), which enhances electrostatic attraction toward negatively charged Cr(VI) species and promotes adsorption as well as interfacial electron transfer. With increasing pH, the dominant Cr(VI) species shifts toward CrO_4^{2-}, which is less reactive toward reduction. Simultaneously, at pH values higher than the pH_{PZC}, the photocatalyst surface becomes negatively charged, leading to electrostatic repulsion between the surface and Cr(VI) anions, thereby suppressing adsorption and photocatalytic activity. Consequently, at pH 10, a substantial decline in Cr(VI) reduction efficiency was observed, confirming that alkaline conditions are unfavorable for the photocatalytic removal of Cr(VI) [48].

The influence of the initial Cr(VI) concentration on the photocatalytic reduction efficiency was tested with five different concentrations: 10, 30, 50, 70, and 90 mg/L; the other conditions were kept constant at pH = 2 and catalyst dose = 0.3 g/L. Fig. 5 c shows that the efficiency of Cr(VI) removal strongly relied on its initial concentration. The highest percentage removal (~97%) was obtained for 10 mg/L after 180 min because lower concentrations favor better contact between Cr(VI) ions and active sites on the photocatalyst surface. However, despite such high efficiency, the absolute amount of chromium removed at this concentration is relatively small. Curiously, for 30 mg/L, the system provided an excellent performance, reaching 93.9% removal, even when the pollutant load increased threefold, indicating that 30 mg/L is probably an optimal concentration where high removal efficiencies are attained for high pollutant loading. Indeed, within the concentration range of 50–90 mg/L, the removal percentage gradually decreased due to saturation of active sites and higher competition among Cr(VI) ions, which decreases the photocatalytic rate. Moreover, for higher concentrations, the solution is more optically dense and restricts light penetration and, therefore, the photon absorption by the catalyst.

To investigate the influence of catalyst dosage on the Cr(VI) reduction efficiency, experiments were carried out using different dosages of the nanocomposite ranging from 0.05 to 0.9 g/L, while keeping the initial Cr(VI) concentration at 30 mg/L and pH at 2. As illustrated in Fig. 5 d, the removal efficiency increased with increasing catalyst dose up to 0.5 g/L, which showed the highest Cr(VI) removal efficiency of 97.5% after 180 minutes. Beyond this dosage, a noticeable decline in performance was observed. The observed trend

J Water Environ Nanotechnol, 2026, 11(4): 491-503
10.22090/jwent.2026.2080911.2032

can be explained based on the availability of active surface area and light penetration. At lower dosages (0.05–0.3 g/L), the number of active photocatalytic sites is limited, which leads to lower reaction rates. As the catalyst dose increases, more active sites become available for Cr(VI) adsorption and reduction, improving photocatalytic activity. However, beyond the optimum point (0.5 g/L), the removal efficiency began to decline. This mostly results from an abundance of catalyst particles that induce light scattering and shielding effects, hence diminishing the effective photon flux that reaches the catalyst surface. Additionally, particle agglomeration at higher concentrations may block active sites and hinder mass transfer of reactants [49].

To investigate the reaction kinetics of Cr(VI) photoreduction using the C-TiO_2/C-g-C_3N_4 nanocomposite, two widely used kinetic models were evaluated: the pseudo-first-order and pseudo-second-order models. As illustrated in Fig. 5 e, the linear plot of $\ln(C_t / C_0)$ versus time yielded a straight line with a high correlation coefficient ($R^2 = 0.99$) and a rate constant of $k_1 = 0.01\,\mathrm{min}^{-1}$. This strong linearity indicates that the Cr(VI) removal process over the nanocomposite fits well with the pseudo-first-order kinetic model, suggesting that the rate-limiting step is likely governed by the availability of active sites on the catalyst surface and the direct interaction of Cr(VI) ions with photogenerated electrons. In contrast, the pseudo-second-order kinetic model was also tested. However, the linear plot of t / C_t versus t, shown in Fig. 5 f, exhibited poor correlation ($R^2 = 0.44$), suggesting that this model does not accurately describe the Cr(VI) photoreduction behavior in this system. From the slope and intercept of the fitted line, the calculated pseudo-second-order rate constant was: $k_2 = 1.215\times10^{-3}\ \mathrm{L\backslash cdotpmg}^{-1}\cdot\mathrm{min}^{-1}$. The low correlation coefficient and inconsistent linearity confirm that the pseudo-second-order model does not appropriately represent the photocatalytic behavior of the system, reinforcing the conclusion that the reaction proceeds primarily via pseudo-first-order kinetics.

The reusability and long-term stability of the C-TiO_2/C-g-C_3N_4 nanocomposite were evaluated over five consecutive photoreduction cycles of Cr(VI) under optimal reaction conditions. As shown in Fig. 5 g, the photocatalytic efficiency gradually decreased from 97.5% in the first cycle (R1) to 75.9% in the fifth cycle (R5). Although a slight decline in performance was observed, the nanocomposite retained a relatively high level of activity, indicating good structural and chemical stability throughout repeated use. The reduction in efficiency over successive runs can be attributed to partial catalyst loss during the recovery process, surface fouling by intermediate by-products, or gradual deactivation of active sites. Despite these minor losses, the C-TiO_2/C-g-C_3N_4 nanocomposite demonstrates promising potential for practical applications due to its acceptable recyclability and photocatalytic robustness.

To understand the photocatalytic mechanism of the

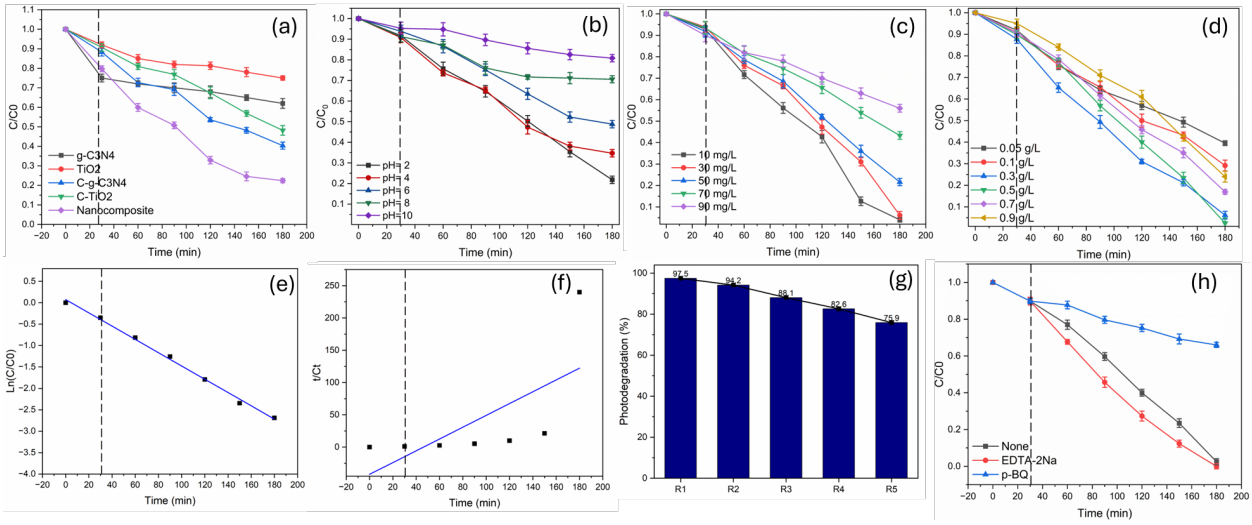


Fig. 5. (a) Photocatalytic reduction of Cr(VI) using different photocatalysts (initial Cr(VI) concentration = 50 mg/L, pH = 2, catalyst dosage = 0.3 g/L), **(b)** effect of solution pH (2-10), **(c)** effect of initial Cr(VI) concentration (10-90), **(d)** effect of catalyst dosage (0.05-0.9), **(e)** pseudo-first-order -kinetic fitting, **(f)** pseudo-second-order kinetic fitting, **(g)** recyclability of the C-TiO_2/C-g-C_3N_4 nanocomposite over five consecutive cycles under optimal conditions, and **(h)** radical scavenger experiments.

Cr(VI) reduction in the case of the C-TiO_2/C-g-C_3N_4 nanocomposite, radical scavenger tests were performed using p-benzoquinone (p-BQ) and EDTA-2Na as quenching agents for photogenerated holes (h^+) and superoxide radicals ($\cdot O_2^-$), respectively. As illustrated in Fig. 5 h, the removal efficiency of Cr(VI) in the absence of any scavenger was 97.5%. Interestingly, in the presence of EDTA-2Na, the photocatalytic efficiency was raised to 100%. Such an enhancement could be explained according to the role of EDTA-2Na as a hole scavenger, since capturing photogenerated holes by EDTA-2Na would inhibit electron-hole recombination, thereby making photoinduced electrons available for the reduction of Cr(VI) to Cr(III). This suggests that the direct participation of holes in the reduction process is not favored, and they act in competition with electrons, where their removal enhances efficiency. On the other hand, in the presence of p-BQ, Cr(VI) removal efficiency took a nosedive, reaching only 34%. The decay of superoxide radicals ($\cdot O_2^-$) by p-BQ attests to the considerable contribution of the $\cdot O_2^-$ species along the path of Cr(VI) photoreduction. This sudden drop in efficiency upon their removal confirms that $\cdot O_2^-$ contributes either directly to the reduction of Cr(VI) or indirectly through generating other reductive species. These observations indicate that the predominant reactive species responsible for Cr(VI) reduction in the present system are superoxide radicals ($\cdot O_2^-$) and photoinduced electrons, whereas photogenerated holes (h^+) are mere recombination centers and do not contribute directly to the reduction process.

The experimental results, along with the findings from radical scavenger experiments, have led to the proposal of a likely mechanism for the photocatalytic reduction of Cr(VI) using the nanocomposite. The C-TiO_2 and C-g-C_3N_4 materials absorb photons upon exposure to visible light, leading to the generation of electron-hole pairs. The suitable band alignment between the two semiconductors facilitates the migration of electrons from the conduction band of g-C_3N_4 to the conduction band of C-TiO_2, hence creating holes in the valence band of g-C_3N_4. This promotes the spatial separation of charge carriers, which diminishes recombination, as evidenced by PL analysis, thereby extending the lifetime of electrons that are available for the reduction reaction. The electrons generated in the conduction band of C-TiO_2 facilitate the direct reduction of Cr(VI) to Cr(III). The electrons may interact with the dissolved oxygen molecules, leading to the formation of superoxide radicals ($\cdot O_2^-$), which play a role in the reduction process as well. The scavenger experiments provide strong evidence that the introduction of p-BQ significantly inhibited the removal of Cr(VI) by functioning as a $\cdot O_2^-$ scavenger. Conversely, the introduction of EDTA-2Na as a hole scavenger led to a remarkable enhancement in the efficiency of Cr(VI) reduction, reaching 100%. This observation indicates that the photogenerated holes serve as recombination centers rather than directly engaging in the reduction process of Cr(VI). Consequently, the C-TiO_2/C-g-C_3N_4 composite structure demonstrates that the collaborative interaction among its components significantly improves charge separation, optimizes the use of photogenerated electrons, and facilitates the generation of reactive oxygen species, all of which contribute to enhanced photocatalytic performance in the removal of Cr(VI).

Comparative Evaluation with Previously Reported Photocatalysts

To further highlight the efficiency and practical relevance of the synthesized C-TiO_2/C-g-C_3N_4 nanocomposite, a

Table 1. Comparative analysis of various photocatalysts for Cr(VI) removal under visible light irradiation.

Photocatalyst	Synthesis Method	Light Source	Optimal Conditions (pH, Cr(VI), Dose)	Removal Efficiency (%)	Time (min)	Ref
TiO_2/Reduced Graphene Oxide Nanocomposite (TiO_2/RGO)	One-step solvothermal method	Visible light	pH = 2; $[Cr(VI)]_0$ = 20 mg/L; dosage = 0.8 g/L	96%	210	[50]
Carbon Dots/TiO_2 Nanostructure Composite (CDs–TNs)	Hydrothermal method	Visible light	pH = 3; $[Cr(VI)]_0$ = 10 mg/L; dosage = 1.0 g/L	100%	150	[51]
$CuBi_2O_4$–TiO_2 Heterojunction	Nitrate method (chemical precipitation)	Solar light	pH = 4; $[Cr(VI)]_0$ = 30 mg/L; dosage = 1.0 g/L	98%	< 240	[52]
Acid/Base-modified g-C_3N_4 (cH-CN and cOH-CN samples)	Chemical surface modification (acidic/alkaline)	Visible light	Optimal acidic pH (≈2–3); initial concentration ≈20 mg/L; high dosage (≥0.5–1.0 g/L)	~100% (within 60 min)	60	[53]
Ternary TiO_2/g-C_3N_4/rGO Nanocomposite (T-CNS-G)	Two-step hydrothermal method	Visible light	pH = 5 (near-neutral); $[Cr(VI)]_0$ = 50 mg/L; dosage = 1.0 g/L (optimal)	≈90%	240	[54]
C-TiO_2/C-g-C_3N_4 (this work)	Hydrothermal	Visible light	pH 2, 30 mg/L, 0.5 g/L	97.5	150	This work

J Water Environ Nanotechnol, 2026, 11(4): 491-503
10.22090/jwent.2026.2080911.2032

comparative analysis with other reported photocatalytic systems for Cr(VI) reduction under visible light is presented in Table 1. The comparison focuses on photocatalyst composition, synthesis method, light source, optimized operating conditions, Cr(VI) removal efficiency, and reaction time. This evaluation not only benchmarks the current material against existing literature but also emphasizes the improvements achieved in terms of simplicity, performance, and cost-effectiveness.

Acknowledgements
The authors express their gratitude to the Babol Noshirvani University of Technology for their generous provision of financial support (BNUT) for the completion of this survey.

Conflict of Interest
The authors declare no conflict of interest. Funding This study was not supported by any funding.

Author's Contributions
Study Conception or Design: KJD; MGH
Data Acquisition: KJD
Data Analysis or Interpretation: KJD; MGH
Manuscript Drafting: KJD
Critical Manuscript Revision: MGH
All authors have approved the final manuscript and are responsible for all aspects of the work.

AI Statement
The authors confirm that no AI tools or services were used during the preparation of this work

CONCLUSION

This study demonstrates the successful development of a fully metal-free carbon-doped TiO_2/g-C_3N_4 nanocomposite as an efficient visible-light-driven photocatalyst for the reduction of toxic Cr(VI) in aqueous media. Comprehensive structural and optical characterizations confirmed the formation of a well-integrated heterojunction with favorable crystallinity, enhanced visible-light absorption, and suppressed electron–hole recombination. The narrowed band gap (2.50 eV), reduced photoluminescence intensity, and stable colloidal dispersion collectively indicate efficient charge separation and transport within the composite structure. Systematic investigation of operational parameters revealed clear optimum conditions for Cr(VI) reduction, namely pH 2, an initial Cr(VI) concentration of 30 mg/L, and a catalyst dosage of 0.5 g/L, under which a maximum removal efficiency of 97.5% was achieved. This performance significantly surpasses that of the individual components, highlighting the strong synergistic interaction between carbon-doped TiO_2 and carbon-doped g-C_3N_4. Kinetic analysis showed that the reduction process follows a pseudo-first-order model (R^2 = 0.99), indicating that surface-mediated electron transfer is the dominant rate-controlling step. Importantly, surface charge analysis revealed a pH_{PZC} value of 5.8, providing a mechanistic explanation for the strong pH dependence of Cr(VI) reduction and confirming that electrostatic attraction under acidic conditions plays a key role in enhancing adsorption and reduction efficiency. Radical scavenger experiments further demonstrated that photogenerated electrons and superoxide radicals ($\cdot O_2^-$) are the primary reactive species responsible for Cr(VI) reduction, while photogenerated holes mainly act as recombination centers. The photocatalyst also exhibited good stability, retaining more than 75% of its initial activity after five consecutive cycles. Overall, the present work highlights the scientific significance of combining simultaneous carbon doping with heterojunction engineering to achieve efficient, stable, and environmentally benign photocatalytic reduction of Cr(VI) under visible light. The findings provide valuable insight into charge-transfer-driven reduction mechanisms and offer a promising, cost-effective strategy for the detoxification of heavy-metal-contaminated wastewater.

REFERENCES

[1] X. Zhang, Y. Zhang, P. Shi, Z. Bi, Z. Shan, L. Ren, The deep challenge of nitrate pollution in river water of China, Science of the Total Environment, 770 (2021) 144674. https://doi.org/10.1016/j.scitotenv.2020.144674

[2] A.M. Lindi, S. Falah, M. Sadeghnezhad, M. Ghorbani, Optimization of fenugreek seed mucilage extraction for the synthesis of a novel bio-nano composite for efficient removal of cadmium ions from aqueous environments, International Journal of Biological Macromolecules, 261 (2024) 129882. https://doi.org/10.1016/j.ijbiomac.2024.129882

[3] D. Sonia, E.K.V. Kirupa, Fabrication of (Ni, S)-Codoped ZnO Nanophotocatalysts as Efficient Solar-Light Driven Photocatalysts for the Degradation of Organic Azo Dyes in Aqueous Media, Journal of Water and Environmental Nanotechnology, 10 (2025) 184-199.

[4] S. Gao, Z. Liu, Q. Yan, P. Wei, Y. Li, J. Ji, L. Li, Facile synthesis of polypyrrole/reduced graphene oxide composite hydrogel for Cr (VI) removal, Journal of Inorganic and Organometallic Polymers and Materials, 31 (2021) 3677-3685. https://doi.org/10.1007/s10904-021-02037-7

[5] Y. Hu, M. Zhi, Z. Zeng, W. Lu, Y. Lai, X. Wang, Efficient removal of Cr (VI) using partially oxidized FeS under visible light, Research on Chemical Intermediates, 48 (2022) 935-948. https://doi.org/10.1007/s11164-022-04657-1

[6] K. Uma, S. Pawar, TiO2/g-C3N4 composites for the removal of chromium in wastewater, Results in Chemistry, 5 (2023) 100743. https://doi.org/10.1016/j.rechem.2022.100743

[7] S. Yanagida, T. Yajima, T. Takei, N. Kumada, Removal of hexavalent chromium from water by Z-scheme photocatalysis using TiO2 (rutile) nanorods loaded with Au core-Cu2O shell particles, Journal of Environmental Sciences, 115 (2022) 173-189. https://doi.org/10.1016/j.jes.2021.05.025

[8] A.M. Lindi, L. Gorgani, M. Mohammadi, S. Hamedi, G.N. Darzi, P. Cerruti, E. Fattahi, A. Moeini, Fenugreek seed mucilage-based active edible films for extending fresh fruit shelf life: antimicrobial and physicochemical properties, International Journal of Biological

Macromolecules, 269 (2024) 132186. https://doi.org/10.1016/j.ijbiomac.2024.132186
[9] X. Yu, R.-Q. Yu, D. Gui, X. Zhang, F. Zhan, X. Sun, Y. Wu, Hexavalent chromium induces oxidative stress and mitochondria-mediated apoptosis in isolated skin fibroblasts of Indo-Pacific humpback dolphin, Aquatic Toxicology, 203 (2018) 179-186. https://doi.org/10.1016/j.aquatox.2018.08.012
[10] B. Kiran, N. Rani, A. Kaushik, Environmental toxicity: exposure and impact of chromium on cyanobacterial species, Journal of Environmental Chemical Engineering, 4 (2016) 4137-4142. https://doi.org/10.1016/j.jece.2016.09.021
[11] N. Madima, K.K. Kefeni, A.T. Kuvarega, S.B. Mishra, A.K. Mishra, Visible-light-driven Z-scheme ternary Fe3O4/TiO2/g-C3N4 nanocomposite as reusable photocatalyst for efficient removal of dyes and chromium in water, Materials Chemistry and Physics, 296 (2023) 127233. https://doi.org/10.1016/j.matchemphys.2022.127233
[12] S. Rawat, N. Misra, M. Singh, M. Tiwari, A. Ghosh, S.A. Shelkar, S. Samanta, N.K. Goel, V. Kumar, Remediation of Cr (VI) using a radiation functionalized green adsorbent: adsorption modelling, mechanistic insights and prototype water purifier demonstration, Journal of Water Process Engineering, 60 (2024) 105109. https://doi.org/10.1016/j.jwpe.2024.105109
[13] C. Yu, Y. Zhu, Y. Yan, Y. Wu, L. Zou, Dual-selective imprinted membrane with asymmetric recognition sites for high-selectivity toward TBBPA and Cr6+ separation, Separation and Purification Technology, 345 (2024) 127402. https://doi.org/10.1016/j.seppur.2024.127402
[14] S. Falah, M. Ghorbani, M. Azimifar, Superamphiphilic Polymeric Coating in Membrane Application: A Mini-Review, Mini-Reviews in Organic Chemistry, 20 (2023) 438-454. https://doi.org/10.2174/1570193X19666220413103855
[15] L. Yu, H. Wang, Q. Huang, H. Liu, Q. Chen, B. Yuan, Q. Li, X. Zhao, J. Tang, D. Zhao, One-pot microwave synthesized high-performance BiVO4/InVO4 heterojunction for photocatalytic reduction of Cr6+, Separation and Purification Technology, 310 (2023) 123143. https://doi.org/10.1016/j.seppur.2023.123143
[16] M. Davarpanah, A. Ahmadpour, T. Rohani Bastami, Preparation and characterization of anion exchange resin decorated with magnetite nanoparticles for removal of p-toluic acid from aqueous solution, Journal of Magnetism and Magnetic Materials, 375 (2015) 177-183. https://doi.org/10.1016/j.jmmm.2014.09.065
[17] (!!! INVALID CITATION !!! [12, 13]).
[18] J.-W. Wang, F.-G. Qiu, P. Wang, C. Ge, C.-C. Wang, Boosted bisphenol A and Cr(VI) cleanup over Z-scheme WO3/MIL-100(Fe) composites under visible light, Journal of Cleaner Production, 279 (2021) 123408. https://doi.org/10.1016/j.jclepro.2020.123408
[19] M.N. Chong, B. Jin, C.W.K. Chow, C. Saint, Recent developments in photocatalytic water treatment technology: A review, Water Research, 44 (2010) 2997-3027. https://doi.org/10.1016/j.watres.2010.02.039
[20] S. Falah, A.M. Lindi, M. Taghavijeloudar, Advancements in Photothermal Materials: Mechanisms, Design, and Sustainable Applications, The first international conference New Approaches in Engineering and Basic Science, 2025.
[21] V. Etacheri, C. Di Valentin, J. Schneider, D. Bahnemann, S.C. Pillai, Visible-light activation of TiO2 photocatalysts: Advances in theory and experiments, Journal of Photochemistry and Photobiology C: Photochemistry Reviews, 25 (2015) 1-29. https://doi.org/10.1016/j.jphotochemrev.2015.08.003
[22] S. N. Ndung'u, E.W. Kinuthia, Kinetics of crystal violet dyes photocatalytic degradation in an aqueous media using TiO2 nanoparticles synthesized from Tithonia diversifolia leaf crude extracts, Journal of Water and Environmental Nanotechnology, 10 (2025) 161-172.
[23] S. Bahrami, A. Ahmadpour, T. Rohani Bastami, A. Ayati, S. Mirzaei, Comparative study of metal nanoparticles anchored TiO2 using polyoxometalate intermediate in photodegradation of azo dye pollutant in aquatic environments, Inorganic Chemistry Communications, 160 (2024) 111986. https://doi.org/10.1016/j.inoche.2023.111986
[24] P. Wang, Y. Li, Z. Liu, J. Chen, Y. Wu, M. Guo, P. Na, In-situ deposition of Ag3PO4 on TiO2 nanosheets dominated by (001) facets for enhanced photocatalytic activities and recyclability, Ceramics International, 43 (2017) 11588-11595. https://doi.org/10.1016/j.ceramint.2017.05.178
[25] L. Lu, G. Wang, M. Zou, J. Wang, J. Li, Effects of calcining temperature on formation of hierarchical TiO2/g-C3N4 hybrids as an effective Z-scheme heterojunction photocatalyst, Applied Surface Science, 441 (2018) 1012-1023. https://doi.org/10.1016/j.apsusc.2018.02.080
[26] Y.-T. Liao, Y.-Y. Huang, H.M. Chen, K. Komaguchi, C.-H. Hou, J. Henzie, Y. Yamauchi, Y. Ide, K.C.-W. Wu, Mesoporous TiO2 embedded with a uniform distribution of CuO exhibit enhanced charge separation and photocatalytic efficiency, ACS applied materials & interfaces, 9 (2017) 42425-42429. https://doi.org/10.1021/acsami.7b13912
[27] M. Neshastehgar, M. Jamshidi, R. Ghamarpoor, Self-assembly TiO2@ Silane@ SiO2 core-shell as s-scheme heterojunction photocatalyst against methylene blue degradation: synthesis and mechanism insights, Journal of Molecular Structure, 1319 (2025) 139406. https://doi.org/10.1016/j.molstruc.2024.139406
[28] I.M. Mohamed, A.G. Shehata, A. Al-Anazi, M. Khairy, E.F. Newair, A template-assisted method for synthesizing TiO2 nanoparticles and Ni/TiO2 nanocomposites for urea electrooxidation, Materials Chemistry and Physics, 316 (2024) 129112. https://doi.org/10.1016/j.matchemphys.2024.129112
[29] J. Tang, J. Li, T. Liu, W. Tang, N. Li, S. Zheng, J. Guo, C. Song, N-doped TiO2-carbon composites derived from NH2-MIL-125 (Ti) for electrochemical determination of tert-butylhydroquinone, Food Analytical Methods, 15 (2022) 2830-2839. https://doi.org/10.1007/s12161-022-02339-7
[30] Y.-Y. Sun, S. Zhang, Kinetics stabilized doping: computational optimization of carbon-doped anatase TiO 2 for visible-light driven water splitting, Physical Chemistry Chemical Physics, 18 (2016) 2776-2783. https://doi.org/10.1039/C5CP07109G
[31] R.S. Ganesh, M. Navaneethan, S. Ponnusamy, C. Muthamizhchelvan, S. Kawasaki, Y. Shimura, Y. Hayakawa, Enhanced photon collection of high surface area carbonate-doped mesoporous TiO2 nanospheres in dye sensitized solar cells, Materials Research Bulletin, 101 (2018) 353-362. https://doi.org/10.1016/j.materresbull.2018.01.018
[32] X. He, M. Wu, Z. Ao, B. Lai, Y. Zhou, T. An, S. Wang, Metal-organic frameworks derived C/TiO2 for visible light photocatalysis: Simple synthesis and contribution of carbon species, Journal of Hazardous Materials, 403 (2021) 124048. https://doi.

org/10.1016/j.jhazmat.2020.124048

[33] Q. Wang, L. Zhang, Y. Guo, M. Shen, M. Wang, B. Li, J. Shi, Multifunctional 2D porous g-C3N4 nanosheets hybridized with 3D hierarchical TiO2 microflowers for selective dye adsorption, antibiotic degradation and CO2 reduction, Chemical Engineering Journal, 396 (2020) 125347. https://doi.org/10.1016/j.cej.2020.125347

[34] S. Zhang, Y. Liu, P. Gu, R. Ma, T. Wen, G. Zhao, L. Li, Y. Ai, C. Hu, X. Wang, Enhanced photodegradation of toxic organic pollutants using dual-oxygen-doped porous g-C3N4: Mechanism exploration from both experimental and DFT studies, Applied Catalysis B: Environmental, 248 (2019) 1-10. https://doi.org/10.1016/j.apcatb.2019.02.008

[35] X. Wang, Y. Ren, Y. Li, G. Zhang, Fabrication of 1D/2D BiPO4/g-C3N4 heterostructured photocatalyst with enhanced photocatalytic efficiency for NO removal, Chemosphere, 287 (2022) 132098. https://doi.org/10.1016/j.chemosphere.2021.132098

[36] A. Mohammad, M.E. Khan, T. Yoon, M. Hwan Cho, Na,O-co-doped-graphitic-carbon nitride (Na,O-g-C3N4) for nonenzymatic electrochemical sensing of hydrogen peroxide, Applied Surface Science, 525 (2020) 146353. https://doi.org/10.1016/j.apsusc.2020.146353

[37] L. Huang, J. Liu, P. Li, Y. Li, C. Wang, S. Shu, Y. Song, CQDs modulating Z-scheme g-C3N4/BiOBr heterostructure for photocatalytic removing RhB, BPA and TC and E. coli by LED light, Journal of Alloys and Compounds, 895 (2022) 162637. https://doi.org/10.1016/j.jallcom.2021.162637

[38] M. Wu, X. He, B. Jing, T. Wang, C. Wang, Y. Qin, Z. Ao, S. Wang, T. An, Novel carbon and defects co-modified g-C3N4 for highly efficient photocatalytic degradation of bisphenol A under visible light, Journal of Hazardous Materials, 384 (2020) 121323. https://doi.org/10.1016/j.jhazmat.2019.121323

[39] W.U. Khan, P. Zhou, L. Qin, A. Alam, Z. Ge, Y. Wang, Solvent-free synthesis of nitrogen doped carbon dots with dual emission and their biological and sensing applications, Materials Today Nano, 18 (2022) 100205. https://doi.org/10.1016/j.mtnano.2022.100205

[40] G. Hosseinzadeh, Synthesis of novel pn heterojunction photocatalyst from ZnO nanorod and Cu2O nanoparticles for degradation of Paraoxon insecticide under visible light irradiation, Journal of Water and Environmental Nanotechnology, 8 (2023) 13-22.

[41] N. Ahmad, C.-F.J. Kuo, M. Mustaqeem, Synthesis of novel CuNb2O6/g-C3N4 binary photocatalyst towards efficient visible light reduction of Cr (VI) and dyes degradation for environmental remediation, Chemosphere, 298 (2022) 134153. https://doi.org/10.1016/j.chemosphere.2022.134153

[42] X. Liu, L. Ma, X. Wang, X. Wu, B. Guo, L. Zhou, Z. Zhao, Structuring dual Z-scheme heterojunction and boosting surface reaction by bifunctional NiCoP modified TiO2/g-C3N4 for improving the photocatalytic activity, International Journal of Hydrogen Energy, 62 (2024) 127-139. https://doi.org/10.1016/j.ijhydene.2024.03.020

[43] Z. Zhao, P. Guo, Y. Zhang, Y. Li, H. Zhang, T. He, S. Li, Fabrication of 2D TiO2/α-Fe2O3/Fe-g-C3N4 heterogeneous from metallurgical solid waste for Photo-Fenton catalysis of levofloxacin/Cr(VI): Electron transfer pathway and DFT calculation, Journal of Catalysis, 432 (2024) 115447. https://doi.org/10.1016/j.jcat.2024.115447

[44] D. Lu, G. Zhang, Z. Wan, Visible-light-driven g-C3N4/Ti3+-TiO2 photocatalyst co-exposed {001} and {101} facets and its enhanced photocatalytic activities for organic pollutant degradation and Cr(VI) reduction, Applied Surface Science, 358 (2015) 223-230. https://doi.org/10.1016/j.apsusc.2015.08.240

[45] A. Surenjan, B. Sambandam, T. Pradeep, L. Philip, Synthesis, characterization and performance of visible light active C-TiO2 for pharmaceutical photodegradation, Journal of Environmental Chemical Engineering, 5 (2017) 757-767. https://doi.org/10.1016/j.jece.2016.12.044

[46] H. Hu, J. Hu, X. Wang, J. Gan, M. Su, W. Ye, W. Zhang, X. Ma, H. Wang, Enhanced reduction and oxidation capability over the CeO 2/gC 3 N 4 hybrid through surface carboxylation: performance and mechanism, Catalysis Science & Technology, 10 (2020) 4712-4725. https://doi.org/10.1039/D0CY00395F

[47] S. Falah, A.M. Lindi, M. Taghavijeloudar, Visible-Light-Driven Photocatalytic Degradation of Basic Yellow Dye Using TiO_2/GO Nanocomposites: A Sustainable Approach to Wastewater Treatment, 8th International Conference on Research in Science & Engineering, 2024.

[48] I.J. Buerge, S.J. Hug, Kinetics and pH dependence of chromium (VI) reduction by iron (II), Environmental science & technology, 31 (1997) 1426-1432. https://doi.org/10.1021/es960672i

[49] S. Falah, M. Ghorbani, J. Ahmadpour, Photocatalytic degradation of anionic and cationic dyes over PPy/CuFe2O4 nanocomposite under visible-light and bactericidal action, Journal of the Taiwan Institute of Chemical Engineers, 144 (2023) 104767. https://doi.org/10.1016/j.jtice.2023.104767

[50] A. Shaikh, S.P. Mishra, P. Mohapatra, S. Parida, One-step solvothermal synthesis of TiO2-reduced graphene oxide nanocomposites with enhanced visible light photoreduction of Cr (VI), Journal of Nanoparticle Research, 19 (2017) 206. https://doi.org/10.1007/s11051-017-3894-7

[51] Y. Li, Z. Liu, Y. Wu, J. Chen, J. Zhao, F. Jin, P. Na, Carbon dots-TiO2 nanosheets composites for photoreduction of Cr (VI) under sunlight illumination: favorable role of carbon dots, Applied Catalysis B: Environmental, 224 (2018) 508-517. https://doi.org/10.1016/j.apcatb.2017.10.023

[52] H. Lahmar, M. Benamira, F. Akika, M. Trari, Reduction of chromium (VI) on the hetero-system CuBi2O4/TiO2 under solar light, Journal of Physics and Chemistry of Solids, 110 (2017) 254-259. https://doi.org/10.1016/j.jpcs.2017.06.021

[53] H. Sun, L. Wang, Y. Liu, Z. Cheng, Y. Zhao, H. Guo, G. Qu, T. Wang, X. Yin, Photocatalytic reduction of Cr (VI) via surface modified g-C3N4 by acid-base regulation, Journal of Environmental Management, 324 (2022) 116431. https://doi.org/10.1016/j.jenvman.2022.116431

[54] G. Li, Y. Wu, M. Zhang, B. Chu, W. Huang, M. Fan, L. Dong, B. Li, Enhanced removal of toxic Cr (VI) in wastewater by synthetic TiO2/g-C3N4 microspheres/rGO photocatalyst under irradiation of visible light, Industrial & Engineering Chemistry Research, 58 (2019) 8979-8989. https://doi.org/10.1021/acs.iecr.8b05990